International Journal of Cardiovascular Medicine and Science, Vol 4, No 2, pp 59-68, 2004

A SHEAR-THINNING VISCOELASTIC FLUID MODEL FOR DESCRIBING THE FLOW OF BLOOD

M Anand, MS, KR Rajagopal, PhD*

Department of Mechanical Engineering, Texas A&M University
College Station, TX 77843 USA

ABSTRACT

A model is developed for the flow of blood, within a thermodynamic framework that takes cognizance of the fact that viscoelastic fluids can remain stress free in several configurations, *ie*, such bodies have multiple natural configurations (see Rajagopal [19], Rajagopal and Srinivasa [20]). This thermodynamic framework leads to blood being characterized by four independent parameters that reflect the elasticity, the viscosity of the plasma, the formation of rouleaus and their effect on the viscosity of blood, and the shear thinning that takes place during the flow. The model emerges in a hierarchy of increasingly complex nonsimple viscoelastic fluid models, and in this study two other models in the same class (proposed by Rajagopal and Srinivasa [20]) are also considered. The efficacy of these models in describing the response of blood is investigated. Among the models studied, the proposed model is not only best able to describe the response of blood but is the first to have rigorous thermodynamic moorings. The predictions of the model agree exceptionally well with the data that is available for steady flow and oscillatory flow experiments, while the two other models are inadequate to describe oscillatory flows (a serious shortcoming as oscillatory flows are the most natural flows that blood undergoes).

The procedure for determining (assigning) the material parameters that characterize blood will be outlined in detail and the results of numerical simulations are compared with the data. This method is also used to fix the relaxation times in the model proposed by Yeleswarapu [39], and the importance of the relaxation times for simulating pulsatile flow is highlighted.

INTRODUCTION

The non-Newtonian behavior of blood manifest in its shear thinning and stress-relaxation properties is well documented. Constitutive modeling of blood has assumed critical importance in the face of increasing evidence that many pathological conditions in the cardiovascular system are influenced in their development and progress by the flow characteristics of blood [10, 13]. The relevance of computational simulations in the development of cardiovascular devices, in particular blood pumps, has been highlighted in a recent article [3], and there is a need for powerful, yet simple, models that can capture the complex rheological response of blood over a range of flow conditions. In this article, we advance a model for blood and investigate its efficacy under conditions of steady and oscillatory flow.

Blood consists in multiple constituents namely red blood cells (RBCs), white blood cells, platelets, *etc*, suspended in a medium (plasma) of proteins and water. The plasma is a Newtonian fluid. The haematocrit (cell matter that consists primarily of RBCs) forms approximately 45% of the volume of normal human blood. Chien, *et al* [4, 5] were among the earliest to relate the shear-thinning nature of blood to the tendency of RBC-rouleau aggregates (which form at low shear) to disaggregate upon the application of shear. Upon increasing the shear rate, the RBCs become '*fluid-like*' and lose their ability to store elastic energy [24]; they also align themselves with the flow field and tend to slide upon plasma layers formed in between [32]. Thurston [27] was among the earliest to recognize the viscoelastic nature of blood, and that the viscoelastic behavior is less prominent with increasing shear rate [28, 31].

In summary, we may state the following about the rheological behavior of blood:

1. It exhibits shear-thinning and responds like a viscoelastic liquid in the shear rates that we are interested in.
2. The RBCs aggregate at low shear rates and are '*solid-like*', being able to store elastic energy. They disaggregate upon application of shear forming smaller rouleau (and later individual RBCs) that are characterized by distinct relaxation times, and which can be subject to further disaggregation although the ease of disaggregation changes (decreases) with rouleau size. At low shear rates, due to the random rouleau network with trapped plasma, dissipation is primarily due to the evolution of the RBC networks, while at high shear rates (small rouleau and individual RBCs in plasma) the dissipation is primarily due to the internal friction. Upon cessation of shear, the material returns to the random rouleau state (entropic behavior). The internal energy is assumed to depend only on the deformation gradient, given the paucity of data on temperature effects. Also, while individual rouleau structures comprise of RBCs stacked in a particular fashion, the entire rouleau network (at the zero-shear state alone) is randomly arranged, and may be assumed to be isotropic with respect to the current natural configuration.

Keywords: *Shear-thinning, viscoelastic fluids, blood flow, modeling, thermodynamic framework, rheological response*

Address for correspondence and reprint request: Dr KR Rajagopal, Department of Mechanical Engineering, Texas A&M University, College Station, TX 77843, E-Mail: Krajagopal@mengr.tamu.edu.
Received 6 January 2003, revised manuscript received 2 December 2003, accepted 9 January 2004.

3. Platelet activation and temperature effects are not considered. The model is developed in an isothermal setting, and the various parameters can be extended to capture the effect of haematocrit on the rheological properties.

One of the earliest to attempt to incorporate the shear-thinning and viscoelastic nature of blood in a single model, Thurston [31] proposed an extended Maxwell model that was applicable to 1-D flow situations. Later, Thurston observed that there exists a critical shear rate beyond which the assumptions of linear viscoelasticity and Newtonian behavior (respectively) of blood cease to hold, and related the non-linear behavior to the microstructural changes that occur in blood with increasing shear rate [33, 34]. The most recent Oldroyd-B type model of Yeleswarapu *et al* [40] is an improvement over earlier proposals like that due to Phillips and Deutsch [16] (see [39] for a detailed literature survey). However, even this model has its limitations given that the relaxation times do not depend on the shear rate, a dependence that can be gleaned from experiments.

A thermomechanical framework for developing models for rate-type fluids has been proposed by Rajagopal and Srinivasa [20], and rate models due to Maxwell, Oldroyd, Burgers, and others are special models within this framework. This approach is well suited for describing bodies whose response functions change as it undergoes deformation. Blood, being such a material, can be modeled within this framework. Importantly, this framework allows for changes in the response of materials due to activation. It has been used to study crystallization [22, 23], and the glass transition phenomenon in polymers [12], for instance. In the future, we intend to incorporate the process of clot formation due to platelet activation in blood flow, the clot being modeled as a viscoelastic fluid or solid (there is some debate on this issue). Additionally, morphological studies of clots have shown certain directional properties due to the fibrin strands that get laid out along the flow direction. Although experimental data for the extent of anisotropy is not available as yet, this framework would be a natural choice to study a transition from a viscoelastic fluid to an anisotropic solid/liquid. In an isothermal setting, the framework involves a choice for the stored energy function and the rate of dissipation. The constitutive relation that is picked maximizes the rate of dissipation amongst the class of models that are possible candidates for the material in question. The assumption that the rate of dissipation is maximized allows us to specify the equation for the evolution of the natural configurations associated with the viscoelastic fluid.

We model blood as a shear-thinning viscoelastic fluid with the relaxation time (characterizing the evolution of natural configurations associated with the fluid) being deformation dependent. This is in keeping with the observation that the viscoelastic character of blood is less prominent with increasing shear rate, and also that the relaxation time characterizing the underlying cellular aggregate at a particular shear rate varies significantly [28, 31].

PRELIMINARIES

The framework for the development of the constitutive theory for viscoelastic fluids (possessing multiple natural configurations) has been outlined in [20], and the notation introduced therein is adhered to here. Let $\kappa_R(B)$ and $\kappa_t(B)$ denote the reference and the current configuration of the body B at time t, respectively. Let $\kappa_{p(t)}(B)$ denote the stress-free configuration that is reached by instantaneously unloading the body, which is at the configuration $\kappa_t(B)$ (Figure 1). As the body continues to deform these natural configurations $\kappa_{p(t)}(B)$ can change (the suffix p(t) is used in order to highlight that it is the preferred stress free state corresponding to the deformed configuration at time t. See Rajagopal [19] for a detailed discussion of the notion of natural configurations).

By the motion of a body we mean a one to one mapping that assigns to each point $\mathbf{X} \in \kappa_R(B)$, a point $\mathbf{x} \in \kappa_t(B)$, for each t, *ie*,

$$\mathbf{x} = \chi_{\kappa_R}(\mathbf{X}_{\kappa_R}, t). \tag{1}$$

We assume that the motion is sufficiently smooth and invertible. We shall, for the sake of convenience, suppress B in the notation $\kappa_R(B)$, *etc.*

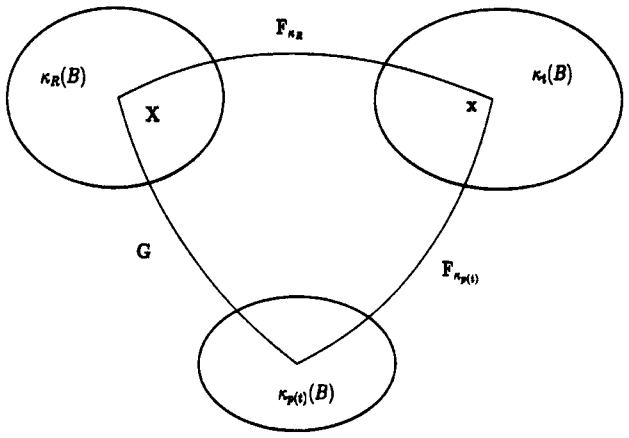

FIGURE 1

Schematic of the natural configurations associated with a viscoelastic fluid having a single relaxation mechanism, and capable of instantaneous elastic response.

The deformation gradients, $\mathbf{F}_{\kappa_R}$, and the left and right Cauchy-Green stretch tensors, $\mathbf{B}_{\kappa_R}$ and $\mathbf{C}_{\kappa_R}$, are defined through:

$$\mathbf{F}_{\kappa_R} = \frac{\partial \chi_{\kappa_R}}{\partial \mathbf{X}_{\kappa_R}}, \ \mathbf{B}_{\kappa_R} = \mathbf{F}_{\kappa_R}\mathbf{F}_{\kappa_R}^T, \text{ and } \mathbf{C}_{\kappa_R} = \mathbf{F}_{\kappa_R}^T\mathbf{F}_{\kappa_R}. \tag{2}$$

The left Cauchy-Green stretch tensor associated with the instantaneous elastic response from the natural configuration $\kappa_{p(t)}$ is defined in like fashion:

$$\mathbf{B}_{\kappa_{p(t)}} = \mathbf{F}_{\kappa_{p(t)}}\mathbf{F}_{\kappa_{p(t)}}^T. \tag{3}$$

The principal invariants of $\mathbf{B}_{\kappa_{p(t)}}$ are

$$\mathrm{I}_{\mathbf{B}} = \mathrm{tr}(\mathbf{B}_{\kappa_{p(t)}}), \ \mathrm{II}_{\mathbf{B}} = \frac{1}{2}\{[\mathrm{tr}(\mathbf{B}_{\kappa_{p(t)}})]^2 - \mathrm{tr}(\mathbf{B}^2_{\kappa_{p(t)}})\}, \text{ and } \mathrm{III}_{\mathbf{B}} = \det(\mathbf{B}_{\kappa_{p(t)}}). \tag{4}$$

For homogeneous deformations, $\mathbf{F}_{\kappa_{p(t)}}$ denotes the deformation gradient between the natural configuration and the current configuration. The mapping $\mathbf{G}$ is defined through:

$$\mathbf{G} = \mathbf{F}_{\kappa_R \to \kappa_{p(t)}} = \mathbf{F}^{-1}_{\kappa_{p(t)}}\mathbf{F}_{\kappa_R}. \tag{5}$$

The velocity gradients, $\mathbf{L}$ and $\mathbf{L}_{\kappa_{p(t)}}$, are defined through

$$\mathbf{L} := \dot{\mathbf{F}}_{\kappa_R}\mathbf{F}^{-1}_{\kappa_R} \text{ and } \mathbf{L}_{\kappa_{p(t)}} = \dot{\mathbf{G}}\mathbf{G}^{-1}, \tag{6}$$

where the dot signifies the material time derivative.

The symmetric parts of $\mathbf{L}$ and $\mathbf{L}_{\kappa_{p(t)}}$, are defined through

$$\mathbf{D} = \frac{1}{2}(\mathbf{L} + \mathbf{L}^T) \text{ and } \mathbf{D}_{\kappa_{p(t)}} = \frac{1}{2}(\mathbf{L}_{\kappa_{p(t)}} + \mathbf{L}^T_{\kappa_{p(t)}}). \tag{7}$$

The upper convected Oldroyd derivative of $\mathbf{B}_{\kappa_{p(t)}}$, $\overset{\nabla}{\mathbf{B}}_{\kappa_{p(t)}}$, is given through

$$\overset{\nabla}{\mathbf{B}}_{\kappa_{p(t)}} = \dot{\mathbf{B}}_{\kappa_{p(t)}} - \mathbf{L}\mathbf{B}_{\kappa_{p(t)}} - \mathbf{B}_{\kappa_{p(t)}}\mathbf{L}^{\mathrm{T}} = -2\mathbf{F}_{\kappa_{p(t)}}\mathbf{D}_{\kappa_{p(t)}}\mathbf{F}^{\mathrm{T}}_{\kappa_{p(t)}}. \tag{8}$$

As we shall assume that blood is incompressible, we shall require that

$$\mathrm{tr}(\mathbf{D}) = 0, \tag{9}$$

and

$$\mathrm{tr}(\mathbf{D}_{\kappa_{p(t)}}) = 0. \tag{10}$$

CONSTITUTIVE ASSUMPTIONS FOR BLOOD

The rate of dissipation ξ associated of the material is defined through

$$\xi = \mathbf{T}\cdot\mathbf{D} - \dot{W}. \tag{11}$$

The form chosen for the rate of dissipation in this study is

$$\xi = \alpha(\mathbf{D}_{\kappa_p(t)}\cdot\mathbf{B}_{\kappa_p(t)}\mathbf{D}_{\kappa_p(t)})^{\gamma} + \eta_1\mathbf{D}\cdot\mathbf{D}. \tag{12}$$

Such a form for the rate of dissipation corresponds to a mixture of a viscoelastic fluid that has a power-law viscosity and a Newtonian fluid. Such a choice is particularly appropriate as blood is a mixture of a Newtonian fluid (plasma) and the other constituents such as cells are elastic membranes containing fluids. The RBC-based microstructure evolves upon the application of shear, the evolution at a particular shear rate depending on the type of rouleau formed (at that shear rate), and becomes progressively liquid-like. While treating blood as a single continuum, we may thus include the entropy production due to the various mechanisms (viscous dissipation and disaggregation of rouleau structures). As a first step, it is assumed that these mechanisms are not interrelated. Additionally, it is assumed that the rate of dissipation is non-negative ($\alpha, \eta_1 > 0$) satisfying the second law.

The Helmholtz potential associated with the elastic response is assumed to be that of a neo-Hookean material[1]:

$$W \equiv \rho\psi = \frac{\mu}{2}(\mathrm{I}_{\mathbf{B}} - 3). \tag{13}$$

Following the procedure of constrained maximisation outlined in [20], the following model (14-18) is obtained[2]:

$$\mathbf{T} = -p\mathbf{1} + \mathbf{S}, \tag{14}$$

$$\mathbf{S} = \mu\mathbf{B}_{\kappa_p(t)} + \eta_1\mathbf{D}, \tag{15}$$

$$\overset{\nabla}{\mathbf{B}}_{\kappa_{p(t)}} = -2(\frac{\mu}{\alpha})^{1+2n}(\mathrm{tr}(\mathbf{B}_{\kappa_{p(t)}}) - 3\lambda)^{n}[\mathbf{B}_{\kappa_{p(t)}} - \lambda\mathbf{1}], \tag{16}$$

$$\lambda = \frac{3}{\mathrm{tr}(\mathbf{B}^{-1}_{\kappa_{p(t)}})}, \tag{17}$$

$$n = \frac{\gamma - 1}{1 - 2\gamma};\ n > 0. \tag{18}$$

The relaxation time governing the evolution of $\mathbf{B}_{\kappa_p(t)}$ is $[2(\frac{\mu}{\alpha})^{1+2n}(\mathrm{tr}(\mathbf{B}_{\kappa_{p(t)}}) - 3\lambda)^{n}]^{-1}$, and is dependent on the elastic stretch. In like fashion, as the shear rate varies, the underlying rouleau size varies as does the corresponding relaxation time. However the relaxation time and the apparent viscosity (as seen from the equations that will be developed shortly) tend to ∞ as $\mathbf{D} \to 0$ (as shear rate tends to zero). This requires some explanation. Earlier, it was believed that blood in the quiescent state exhibited a yield-stress behavior[3]; the once popular Casson model reflects this idea as does the more recent model of Sun and DeKee [26]. However, there is the possibility that the difficulty in measuring viscosity at low shear rates might be at the root of the assumption that $\mu_{app} \to \infty$ as shear rate tends to zero (see [7]). In order to ensure that the zero-shear viscosity is finite, we introduce a Heaviside function into the expressions for the viscosity and shear thinning index,

$$\alpha = \alpha_f \mathrm{H}(\mathrm{I}_{\mathbf{B}} - \mathrm{I}_0) + \alpha_0(1 - \mathrm{H}(\mathrm{I}_{\mathbf{B}} - \mathrm{I}_0)), \tag{19}$$

$$\gamma = \gamma\mathrm{H}(\mathrm{I}_{\mathbf{B}} - \mathrm{I}_0) + (1 - \mathrm{H}(\mathrm{I}_{\mathbf{B}} - \mathrm{I}_0)), \tag{20}$$

$$\alpha_0 = 2(\eta_0 - \eta_\infty), \tag{21}$$

where η_0, η_∞ are the asymptotic viscosities of blood at low and high shear rates, and I_0 is a suitably chosen constant. We shall find it convenient to introduce the notation

$$\mathrm{K} = (\frac{\mu}{\alpha})^{1+2n}. \tag{22}$$

OTHER CONSTITUTIVE MODELS

Different choices for the rate of dissipation in Equation (11) lead, of course, to different models. In particular, the models proposed in [20] are also studied to examine their relevance *vis-a-vis* modeling blood flow. The Generalized Oldroyd-B (GOB) model developed by Rajagopal and Srinivasa [20] has the following form:

$$\mathbf{T} = -p\mathbf{1} + \mathbf{S}, \tag{23}$$

$$\mathbf{S} = \mu\mathbf{B}_{\kappa_{p(t)}} + \eta_1\mathbf{D}, \tag{24}$$

$$\mathbf{S} + \frac{\eta}{2\mu}\overset{\nabla}{\mathbf{S}} = \eta_1(\mathbf{D} + \tfrac{\eta}{2\mu}\overset{\nabla}{\mathbf{D}}) + \mu\lambda\mathbf{1}, \tag{25}$$

$$\lambda = \frac{3}{\mathrm{tr}(\mathbf{B}^{-1}_{\kappa_{p(t)}})}. \tag{26}$$

A related model, the Generalized Maxwell (GM) model is, unlike the Generalized Oldroyd-B model, capable of an instantaneous elastic response. The equations for this model are:

$$\mathbf{T} = -p\mathbf{1} + \mathbf{S}, \tag{27}$$

[1] It is only the rouleau network at zero-shear that is randomly arranged. The underlying rouleau formations at higher shear rates consist of RBCs arranged in a certain fashion. Thus, if the underlying microstructure is related to the elastic response, although the configuration is initially isotropic, it evolves into one whose stress-free state is not. Directional effects may thus come into play, and it would be interesting to see if morphological observations that seem to point to a possible transverse isotropy in the underlying elastic response can be confirmed through a suitably designed experiment. Rajagopal and Srinivasa [21] point out that the effects of anisotropy may be important in the context of an isotropic fluid infused with rod-like suspensions and these issues may be of critical importance in whole blood given that 45% by volume is cell matter.

[2] This model is not capable of an instantaneous elastic response. See discussion in [20].

[3] While one often finds the assumption of a yield condition for certain fluids that are referred to as Bingham fluids the notion of yield is counter to what is meant by a fluid. A body is said to be a fluid if it cannot sustain a shear. Thus, a fluid will flow, however small the shear stress. While the flow might not be perceptible for short times, given sufficient time it will be perceptible. Thus, it is not meaningful to allow fluids to have a yield-stress (see Murali Krishnan and Rajagopal [15] for a discussion of this issue).

$$\mathbf{S} = \mu \mathbf{B}_{\kappa_{p(t)}}, \tag{28}$$

$$\overset{\nabla}{\mathbf{B}}_{\kappa_{p(t)}} = -2\frac{\mu}{\eta}[\mathbf{B}_{\kappa_{p(t)}} - \lambda \mathbf{1}], \tag{29}$$

$$\lambda = \frac{3}{\mathrm{tr}(\mathbf{B}^{-1}_{\kappa_{p(t)}})}. \tag{30}$$

It has been shown that the above models can be reduced to, or expressed equivalently, in the manner of the classical Oldroyd-B and upper-convected Maxwell models [20]. While the models given above have a thermodynamic basis, the model proposed by Yeleswarapu [39] does not.

The model proposed by Yeleswarapu [39] is a generalization of the Oldroyd-B model which was obtained by fitting the model to experimental data. He showed that this model seemed to fit the data better than the models that were being used at that time. The constitutive equation for this model is as given below:

$$\mathbf{T} = -p\mathbf{1} + \mathbf{S}, \tag{31}$$

$$\mathbf{S} + \lambda_1\left(\dot{\mathbf{S}} - \mathbf{LS} - \mathbf{SL}^{\mathrm{T}}\right) = \nu(\mathbf{A}_1)\,\mathbf{A}_1 + \eta_0\lambda_2\left(\mathbf{A}_1 - \mathbf{LA}_1 - \mathbf{A}_1\mathbf{L}^{\mathrm{T}}\right), \tag{32}$$

where $\nu(\mathbf{A}_1)$ is given by the following:

$$\nu(\mathbf{A}_1) = \eta_\infty + (\eta_0 - \eta_\infty)\left[\frac{1 + \ln(1 + \Lambda\dot{\gamma})}{1 + \Lambda\dot{\gamma}}\right], \tag{33}$$

$$\dot{\gamma} = \left[\frac{1}{2}\mathrm{tr}(\mathbf{A}_1^2)\right]^{1/2}. \tag{34}$$

CORROBORATION OF MODEL

We will now discuss the efficacy of the model that has been developed here, namely the model defined through Equations (14)-(18). The parameters K, μ, n and η_1, that are used in defining the model (Equations (14) - (18)) are determined so that the best fit is obtained for both steady flow data [39] and oscillatory flow data [29]. The model is corroborated by comparing predictions with the data for steady Poiseuille flow [40]. In our numerical procedures, we treat the model without reference to Equations (19)-(21). This is a minor detail, and relates to setting I_0 to correspond to the value of I_B at the lowest shear rate (in the measurement of apparent viscosity). The value of K would then be used to infer α_f. There is little difference in the results presented if Equations (19)-(21) are required to be met. For instance, we find that I_0 = 3.0006 for the data on human blood (for a lowest measurable shear rate of 0.06 sec^{-1}), and I_B almost never reaches this value in our numerical simulations. Applications that demand numerical results of high fidelity should however solve the full system of equations along with data that report the apparent viscosity at even lower shear rates.

APPARENT VISCOSITY

Apparent viscosity data has been obtained for the steady flow of blood in the rotating cylinder rheometer [39] by correlating the solutions calculated from the theory. The material constants are inferred from measurements of torque and shear rate. We note that most commercial cylindrical rheometers (like the one used to obtain the data in [39]) employ a data reduction procedure based on a "small gap" assumption (see [37]). These approximate the shear rate at the wall by a constant mean value assuming that the variation of shear rate across the gap is small. The validity of such an assumption is questionable for non-Newtonian liquids (see Yeleswarapu [39] for a brief parametric study of his model in such a flow situation). However, we shall proceed by assuming that the measured shear rate is a good approximation to the wall shear rate. It is preferable to use data (if available) reporting measured torques (or wall shear stresses) and angular speeds so that the intervening approximations may be reduced, and the material parameters may be fixed with greater precision. Data in the literature that has been reviewed is reported as apparent viscosity, though.

The flow field between the cylinders is assumed to be of the following form:

$$\mathbf{v} = u(r)\hat{\mathbf{e}}_\theta = rw(r)\hat{\mathbf{e}}_\theta \tag{35}$$

Substituting the constitutive equations (14)-(18) in the equations for balance of linear momentum and assuming an axisymmetric two dimensional stress field, the following expression is obtained for the wall shear stress (from which the torque is calculated):

$$T_{r\theta} = \left(\frac{\frac{\mu\lambda}{\chi} + \eta_1}{2}\right)\left(\frac{du}{dr} - \frac{u}{r}\right). \tag{36}$$

Assuming that the shear rate is nearly constant across the gap ("thin gap assumption"), we obtain:

$$\frac{du}{dr} - \frac{u}{r} = R_o\frac{\Delta w}{\delta r}, \tag{37}$$

where R_0 is the radius of the outer cylinder, Δw is the difference in angular velocity between the outer and inner rotating cylinders, and δr represents the gap between the cylinders. The apparent viscosity that will be reported for the model, given the torque and the shear rate, is:

$$\mu_{app} = \frac{\frac{\mu\lambda}{\chi} + \eta_1}{2}, \tag{38}$$

where λ is determined using the incompressibility condition: $det(\mathbf{B}_{\kappa_{p(t)}}) = 1$, and it is given by:

$$\lambda = \frac{1}{\left[1 + \frac{1}{4\chi^2}\left(\frac{du}{dr} - \frac{u}{r}\right)^2\right]^{1/3}}. \tag{39}$$

At any given shear rate, χ is obtained by solving:

$$\chi = \mathrm{K}\left[\frac{2\dot{\gamma}_{meas}^2}{4\chi^2}\frac{1}{(1 + \frac{\dot{\gamma}_{meas}^2}{4\chi^2})^{1/3}}\right]^n, \tag{40}$$

where

$$\dot{\gamma}_{meas} = \left(\frac{du}{dr} - \frac{u}{r}\right). \tag{41}$$

We may fix all four parameters using the above expressions (Equations (38),(39),(40)). For the limit $\dot{\gamma}_{meas} \to 0$, we find that $\lambda \backslash \chi \to \infty$, though this can be fixed using Equations (19-21). For the limit $\dot{\gamma}_{meas} \to \infty$, $\lambda \backslash \chi = 0$ and $\eta_1 = 2\eta_\infty$. The multidimensional unconstrained minimisation procedure in MATLAB (fminsearch) is used to fix K, μ and n for the best fit, with χ being solved by the fzero routine in MATLAB. The constants obtained (for human blood: $\eta_0 = 0.0736 Pa.s$, $\eta_\infty = 0.005 Pa.s$, $\Lambda = 14.81 s$) are K=58.0725 s^{-1}, μ = 0.1611 N/m^2, n = 0.5859 (n must be positive to ensure shear-thinning behavior), and η_1 = 0.01 $Pa.s$, and are but one among a very large selection that can fit the data equally well. It is seen that the proposed model fits the experimental data better than the model proposed by Yeleswarapu at shear rates higher than 1 sec^{-1} (Figure 2).

The corresponding expressions for apparent viscosity from the other models are:

$$\mu_{app}(GOB) = \frac{\eta\lambda + \eta_1}{2}, \tag{42}$$

$$\mu_{app}(GM) = \frac{\eta\lambda}{2}, \tag{43}$$

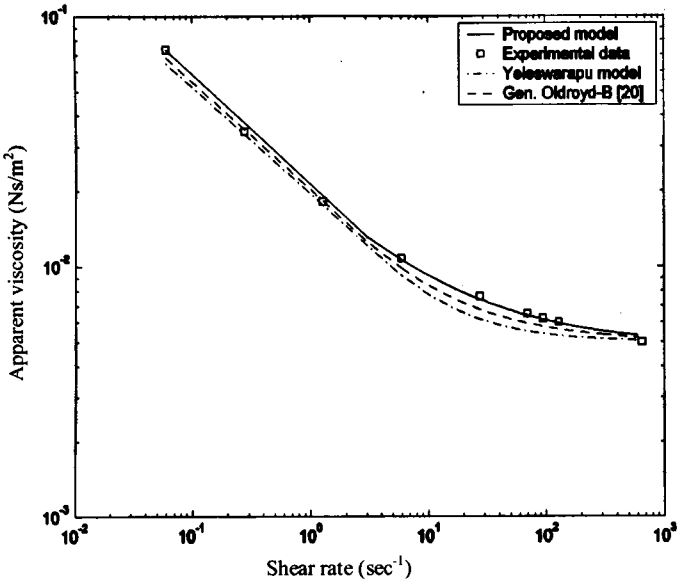

FIGURE 2

Apparent viscosity of blood. Predictions (of μ_{app}) using the proposed model, the GOB model, and the Yeleswarapu model are compared with the data for human blood ([39]).

$$\lambda = \frac{1}{\left[1 + \frac{1}{\kappa^2}\left(\frac{du}{dr} - \frac{u}{r}\right)^2\right]^{1/3}}. \tag{44}$$

Here $\kappa = 2\mu/\eta$, and μ refers to the elastic shear modulus in the corresponding models. Next, λ is obtained using the incompressibility condition: $det(\mathbf{B}_{\kappa_{p(t)}}) = 1$. The expression for the apparent viscosity for Yeleswarapu's model is as follows:

$$\mu_{app}(Yel) = \nu(\dot{\gamma}_{meas}), \tag{45}$$

where $\dot{\gamma}$ in Equation (33) is found to be $\dot{\gamma}_{meas}$. The apparent viscosity expression for the Generalized Oldroyd-B model, like the Yeleswarapu model, tends to asymptotic values at zero and infinite shear rates (when λ is 1 and 0, respectively). These are set to correspond to the asymptotic viscosities for the sample of blood that is tested. Therefore, $\eta_1 = 2\eta_\infty$ and $\eta = 2(\eta_0 - \eta_\infty)$. The (elastic) shear modulus μ in the GOB model is fixed by a least squares fit to the experimental data. The Generalized Maxwell model cannot capture the asymptotic non-zero viscosity at infinite shear rates. We can only fix $\eta = 2\eta_0$ letting the value at infinite shear rate to become zero. The graphs of the various expressions for μ_{app} are shown in Figure 2. It is seen that the GOB model gives as good a fit as the generalized viscosity function in the Yeleswarapu model. The constants in GOB for the data in Figure 2 are $\mu = 0.0077$ N/m^2, $\eta = 0.1372$ *Pa.s* , and $\eta_1 = 0.01$ *Pa.s* .

APPLICATION TO STEADY POISEUILLE FLOW

The experimental set up is described in detail by Yeleswarapu, *et al* [40]. The equations for steady axisymmetric flow (in dimensional form) are solved numerically, for a specified mean flow velocity (V_{mean}). We use the iterative solvers for non-linear algebraic equations (fsolve, fzero) available in MATLAB.
The following equations are solved:

$$\frac{du}{dr} = \frac{\partial p'}{\partial z}\frac{r}{\left(\frac{\mu\lambda}{\chi} + \eta_1\right)}, \tag{46}$$

$$\frac{\partial p'}{\partial z} = \frac{-R_{pipe}^2 V_{mean}}{\int_0^{R_{pipe}} \frac{r^3}{\left(\frac{\mu\lambda}{\chi} + \eta_1\right)} dr}, \tag{47}$$

subject to the no-slip boundary condition and the centerline maximum condition. (Note that p' represents the appropriate pressure term in the model: p-$\mu\lambda$). We solve for du/dr, at each r, that satisfies the above two equations and the centerline maximum condition. Using the values of du/dr and u (R_{pipe} = 1) = 0 (No-slip), the velocity profile can be constructed. The above equations are solved iteratively till dp'/dz is accurate (relative) to within $\varepsilon = 10^{-4}$.

For the other three models, the following equations are solved:

$$\frac{du}{dr} = \frac{\partial p'}{\partial z}\frac{r}{2\mu_{app}}, \tag{48}$$

$$\frac{\partial p'}{\partial z} = \frac{-R_{pipe}^2 V_{mean}}{\int_0^{R_{pipe}} \frac{r^3}{2\mu_{app}} dr}, \tag{49}$$

Note that p' represents the appropriate pressure term in the model: p- $\mu\lambda$ for GOB and GM, and p for the Yeleswarapu model.

The predictions of the (proposed) model agree well with the experimental data (Figure 3). The overall accuracy is around the same for both the model proposed here and that proposed by Yeleswarapu. Table 1 summarizes the results. K = 0.3845s^{-1}, μ = 0.0667N/m^2, n = 0.2998 and $\eta_1 = 0.013$ *Pa.s* gives a good fit to the apparent viscosity data for porcine blood [40] (η_0=0.2*Pa.s* , η_∞=0.0065*Pa.s* , Λ=11.14*s*). A good match is also obtained with the Generalized Oldroyd-B model (μ = 0.0388N/m^2, η = 0.387 *Pa.s* , η_1 = 0.013 *Pa.s*), though not with the Generalized Maxwell model.

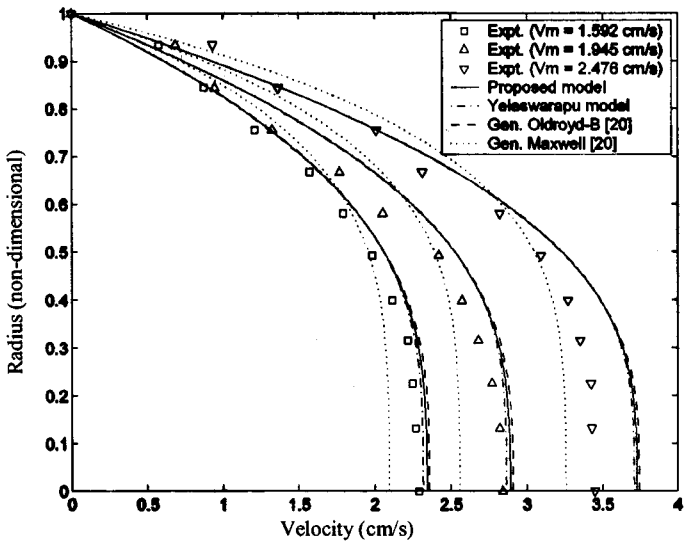

FIGURE 3

Velocity profiles: Theoretical predictions, for Poiseuille flow, using the proposed model, the GOB model, and the GM model, are compared with the data for porcine blood ([40]).

APPLICATION TO OSCILLATORY FLOW

The model parameters are fixed so that the amplitude of and phase difference between the pressure gradient and volume flow rate predicted through a numerical simulation matches the experimental

data for a set of cases. This procedure has not been adopted hitherto[4], and is essential to validate the model over the gamut of flow conditions that are expected in the human vasculature (such a study of Yeleswarapu's model reveals a shortcoming of the model).

TABLE 1
Comparison of models' predictions (of centerline velocity) with data [40] for Poiseuille flow of porcine blood

Case	Measured	Ref [40]	Proposed Model	GOB	GM
	cm/s	cm/s	cm/s	cm/s	cm/s
I	2.30	2.32 (0.90%)	2.341 (1.83%)	2.36 (2.61%)	2.10 (8.70%)
II	2.84	2.87 (1.00%)	2.888 (1.69%)	2.90 (2.11%)	2.56 (9.86%)
III	3.44	3.70 (7.50%)	3.725 (8.28%)	3.74 (8.72%)	3.26 (5.23%)

Thurston has proposed a method of inferring the complex compliances (this presumes that the model is that of a linear viscoelastic material) from measurements of the pressure gradient and volume flow (and the phase difference between them) in oscillatory and pulsatile flow through small tubes ([29], [30]). The pressure gradient in phase with the volume flow rate (P′), and the component in quadrature with the volume flow rate (P") are measured along with the (amplitude of) volume flow rate, and these are used to infer the values of the complex compliances (η', η"; see [37] for an explanation of these quantities). Such a data reduction procedure is not correct, given that we are dealing with a non-linear viscoelastic fluid; the pressure gradient and volume flow rate values from the numerical simulations are thus compared with the values of pressure gradient and volume flow rate reported in [29]. Experimental data at frequencies of 2 Hz and 0.5 Hz, though as complex compliances, has been reported for a similar set-up in [32] and [35] respectively. There are other procedures by which the compliances may be inferred (see [36, 37]), and these too have been reported in the literature [6,35]. All such data reduction presupposes that the fluid is a linearly viscoelastic fluid.

We seek a solution for oscillatory flow in a pipe of the form:

$$\mathbf{v} = u(r,t)\hat{e}_z\,;\; p = p(r,z,t). \tag{50}$$

A time periodic solution is sought for $\mathbf{V}$, given the time periodicity of the imposed pressure gradient:

$$-\frac{1}{\rho}\frac{\partial p}{\partial z} = A\cos(wt). \tag{51}$$

Upon substituting Equations (50) and (51) into the balance of linear momentum, we obtain (in non-dimensional form), on assuming that the components of the stress depend only on the radial coordinate, that:

$$\frac{\partial u^*}{\partial t^*} = -\frac{\partial p^*}{\partial z^*} + \frac{S^*_{rz}}{r^*} + \frac{\partial S^*_{rz}}{\partial r^*}, \tag{52}$$

$$\frac{\partial B_{rz}}{\partial t^*} = \frac{\partial u^*}{\partial r^*}B_{rr} - 2\chi(B_{\kappa_{p(t)}})\frac{R}{\mathrm{Ve}}B_{rz}, \tag{53}$$

$$\frac{\partial B_{rr}}{\partial t^*} = 2\chi(B_{\kappa_{p(t)}})\frac{R}{\mathrm{Ve}}(\lambda - B_{rr}), \tag{54}$$

$$\frac{\partial B_{zz}}{\partial t^*} = 2\frac{\partial u^*}{\partial r^*}B_{rz} + 2\chi(B_{\kappa_{p(t)}})\frac{R}{\mathrm{Ve}}(\lambda - B_{zz}), \tag{55}$$

[4] Chmiel and Walitza [7] check the predictions of their model with such data over a smaller range, but use an incorrect procedure to determine the parameters.

where

$$S^*_{rz} = \frac{\mu}{\rho \mathrm{Ve}^2}B_{rz} + \frac{\eta_1}{2\rho R\,\mathrm{Ve}}\frac{\partial u^*}{\partial r^*}, \tag{56}$$

$$\lambda = \frac{3B_{rr}\left(B_{rr}B_{zz} - B_{rz}^2\right)}{B_{rr}^2 + 2B_{rr}B_{zz} - B_{rz}^2}, \tag{57}$$

$$\chi(B_{\kappa_{p(t)}}) = K\left(2B_{rr} + B_{zz} - 3\lambda\right)^n. \tag{58}$$

and R, Ve are the pipe radius and characteristic velocity respectively. (Note: $B_{\theta\theta} = B_{rr}$, $B_{r\theta} = B_{\theta z} = 0$).

We use the following non-dimensionalisation: $t^* = t\mathrm{Ve}/R$, $w^* = wR/\mathrm{Ve}$, $u^* = u/\mathrm{Ve}$, $r^* = r/R$, $z^* = z/R$, $S_{rz}^* = S_{rz}/\rho\mathrm{Ve}^2$, $p^* = p/\rho\mathrm{Ve}^2$, and $A^* = AR/\mathrm{Ve}^2$.

The above PDEs are solved over the domain $0 < r < 1$, for $t \geq 0$, subject to the following boundary condition:

$$u^*(1,t) = 0, \tag{59}$$

and center-line condition:

$$\frac{\partial u^*(0,t)}{\partial r^*} = 0. \tag{60}$$

We use the exact solution for pulsatile flow of a Newtonian fluid [33] as the initial condition.

A predictor-corrector type numerical approach is used to solve these equations. The (coupled) PDEs are decoupled from each other, and the PDE for the velocity is treated as an IBVP, while the others are treated as IVPs. The coupling is brought about by means of an iterative process at each time step. The absence of the spatial derivative for B_{rz}, *etc*, (the components of $\mathbf{B}_{\kappa_{\mathbf{p}}(t)}$) in the appropriate equations, implies that it is enough to fix the boundary conditions for the velocity. Once the velocity is obtained, the values of the components of $\mathbf{B}_{\kappa_{\mathbf{p}}(t)}$ can be obtained over the entire domain $(0 \leq r \leq 1)$.

The algorithm used is as follows:

1. Compute $y_{k+1}^{(0)}$ using $y_{k+1}^{(0)} = y_k + \Delta t\, f(t,y_k)$
(where $\partial y/\partial t = f(t,y)$)
2. Compute $y_{k+1}^{(m)}$ (m=1, 2,...) using:
$$y_{k+1}^{(m)} = y_k + 0.5\Delta t\left[f(t,y_k) + f(t+\Delta t, y_{k+1}^{(m-1)})\right]$$
3. Carry out the iteration until relative error between consecutive iterates is less than $\varepsilon = 10^{-4}$, for all variables.

Here y_k denotes the general variable (u, B_{rz}, *etc*) at the corresponding instant of time, $t = k\Delta t$. For the variable u, we obtain the values on the nodes (2 to n-1), and apply the boundary conditions (centerline maxm. with a finite difference scheme of appropriate accuracy, and no-slip). For the variables B_{rz}, *etc*, we use the above scheme on all the nodes including those on the boundary. Natural cubic splines are used to approximate the spatial derivatives in these equations [9]. The scheme is $\Theta((\Delta t)^2, (\Delta r)^2)$, and simulations are done with $\Delta t = 2\times10^{-4}$ and $\Delta r = 0.05$. Computations proceed until a periodic solution is obtained. The solution sought permits no axial dependence for the stress components, and the extra normal stress is numerically verified to have little variation in the radial direction.

The numerical simulations are performed ($\rho = 1053.6\mathrm{kg/m}^3$, Ve = 1cm/sec) for a pipe of radius, R = 0.43 mm, at a frequency, f = 2Hz, in like manner to the experiments. How the predictions of the theory match the experimental data is depicted in Figures 4 and 5 for two choices of parameters, both of which fit the apparent viscosity data exceptionally well. However, there is one complication here: the values of K, μ, n that are optimal for fitting the oscillatory flow data may not fit the apparent viscosity data equally well. We cannot have

different values of K, μ, n, *etc* for different flows and thus we need to pick a single set of values that fit a range of experiments adequately. We thus have a combined optimization problem with a least squares objective function involving three parameters and two systems of equations (non-linear algebraic equations for μ_{app} and PDEs for oscillatory flow) as constraints. The fit shown can be made better through better optimization procedures, but we shall not adopt elaborate techniques here given the convergence characteristics of the numerical procedures adopted. Our aim is to focus on a method to corroborate the viscoelastic models for blood, and to show that the agreement with experiments can be improved by working in a reasonable range of the parameters.

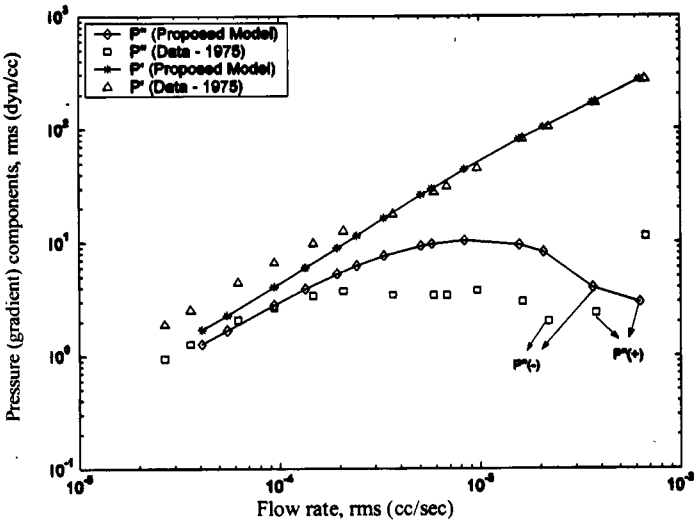

FIGURE 4

Pressure (gradient) components in phase, P′, and in quadrature, P", with (amplitude of) volume flow rate. The predictions of the proposed model (K = 5.2908 s^{-1}, μ = 0.053 N/m^2, n = 0.5925, and η_1 = 0.01 Pa.s), are compared with the data for Human blood ([29]).

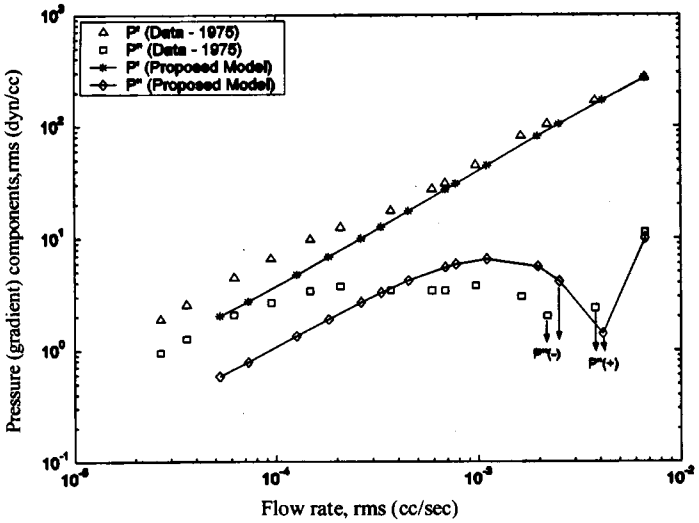

FIGURE 5

Pressure (gradient) components in phase, P′, and in quadrature, P", with (amplitude of) volume flow rate. The predictions of the proposed model (K = 1.2056 s^{-1}, μ = 0.0227 N/m^2, n = 0.7525, and η_1 = 0.01 Pa.s), are compared with the data for Human blood ([29]).

A similar procedure for the GOB model and the Yeleswarapu model leads to the results shown in Figures 6 and 7. The GOB model offers little freedom to match data (since the parameters are uniquely determined from the data on apparent viscosity), whereas the two parameters of Yeleswarapu's model can be adjusted to match the data. The non-dimensionalised PDEs for Yeleswarapu's model are given in [17], and they are solved using the numerical procedure already outlined. The relaxation times used in [17] do not satisfy the usual constraint for the Oldroyd-B model namely that $\lambda_1 > (\lambda_2\eta_0/\eta_\infty)$. A simple Gauss-Newton method[5] is used to find the range of λ_1 and λ_2 which gives the best agreement with data. The results (for λ_1 = 0.1530 s, λ_2 = 0.0101 s) fit the experimental data (for human blood) quite well.

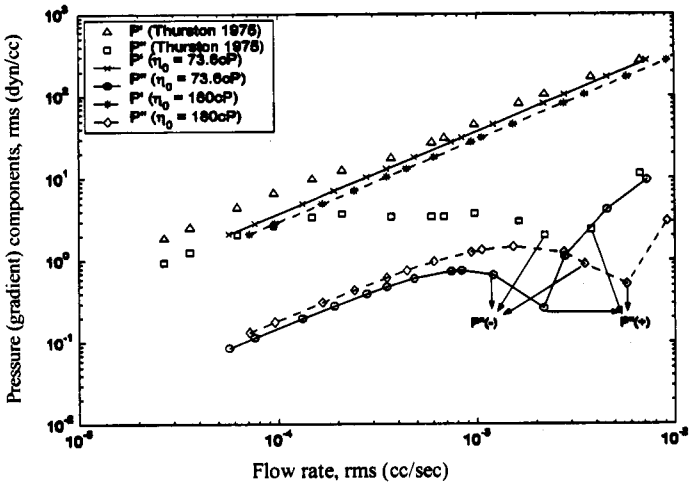

FIGURE 6

Pressure (gradient) components in phase, P′, and in quadrature, P", with (amplitude of) volume flow rate. The predictions of the GOB model [20], are compared with the data for human blood ([29]) (η = 0.35208 Pa.s, η_1 = 0.00792 Pa.s, μ = 0.0083 N/m^2 in GOB for η_0 = 180 cP).

Interestingly, for this set of relaxation times, Yeleswarapu's model[6] predicts flow reversals for a pulsatile pressure gradient of the form:

$$-\frac{1}{\rho}\frac{\partial p}{\partial z} = A\left(1+\cos(wt)\right) \tag{61}$$

the (relative) magnitude of flow reversal decreasing with increasing amplitude of the pressure gradient (Figure 8, see Table 2). This is a corroboration of the experimental evidence that the elastic properties of blood become less prominent with an increase in shear rate; inertial effects being more important at higher shear rates, and elastic effects dominating at low shear rates. It would be interesting to demonstrate this experimentally and to report the actual extent of flow reversal. However, no such data is available at the moment. A similar study with the Classical Oldroyd-B model ($\eta_0 = \eta_\infty = 0.01\ Pa.s$, λ_1 = 0.1530 s, λ_2 = 0.0101 s) shows that the extent of flow reversal is a constant. Table 2 gives a clearer picture of this result (ρ = 1050kg/m^3, R = 0.5 mm, Ve = 1mm/sec, and f = 2Hz, for this set of simulations).

The set of experimental data we have used is just one among the many that can be used to infer and corroborate the viscoelastic nature

[5] Although it is possible that one or even a few sets of values can be matched by two combinations of the relaxation times, there is only one choice of λ_1, λ_2 which yields the best fit for the entire set.

[6] This result is obtained for the proposed model also.

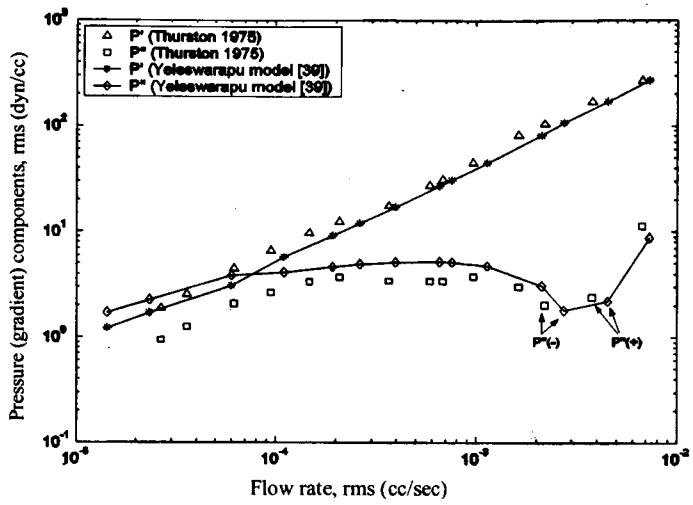

FIGURE 7

Pressure (gradient) components in phase, P′, and in quadrature, P", with (amplitude of) volume flow rate. The predictions of the Yeleswarapu model [39] (λ_1=0.1530 s, λ_2=0.0101 s), are compared with the data for human blood ([29]).

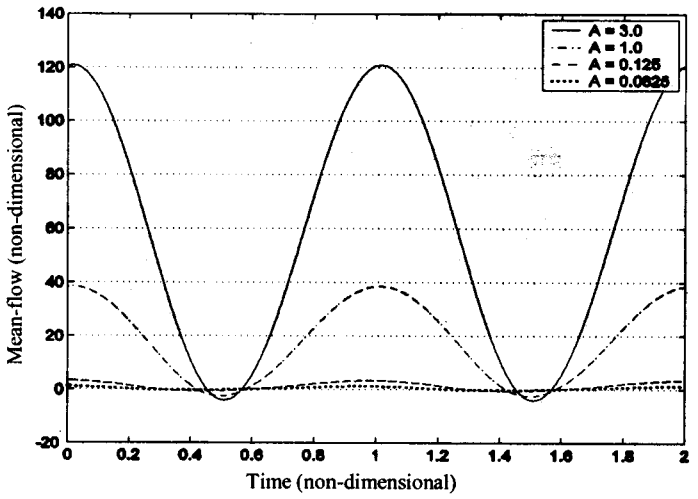

FIGURE 8

Mean flow (and reversal) for various (non-zero mean (Equation (61))) pressure gradients for λ_1=0.1530 s, λ_2=0.0101 s.

TABLE 2

Flow reversal (non-dimensional) with the Yeleswarapu [39] (Yele) and Classical Oldroyd-B (Old-B) models

A	Flow reversal/cycle		Mean flow/cycle		Extent of reversal/cycle	
	Yele [39]	Old-B	Yele [39]	Old-B	Yele [39]	Old-B
3.0	0.2959	9.9911	58.4778	30.8307	0.51%	32.41%
1.0	0.2487	3.3304	18.3001	10.2769	1.38%	32.41%
0.125	0.0965	0.4163	1.4421	1.2846	7.17%	32.41%
0.0625	0.0420	0.2081	0.4811	0.6424	9.57%	32.39%

of blood. Some of the experiments that need to be mentioned in this regard are the hysteresis experiments, among others, by Bureau, *et al* [1, 2]. These experiments are mentioned in [26], and can be verified for the model proposed here. Other experiments include the stress (formation and)-relaxation data due to Joly, *et al* [11] and McMillan, *et al* [14] (see Quemada [18]). Both sets of data can be explained using the model proposed here (see [21] for shear stress variation (with time) from the moment of imposition of a steady shear flow, for an anisotropic fluid). The usefulness of a similar model, for stress-relaxation data (upon sudden cessation of steady shear flow), is illustrated in [25], and in this case (unlike the data in [25]) there is no uncertainty in the initial state of strain. In all the above cases (as apart from the set of data we have studied which involved an IBVP), we need to solve an IVP involving a coupled system of PDEs, and the parameters will have to be adjusted so that the solution of this IVP matches the experimental data. There is no data for the normal stress differences for the flow of blood, and Copley and King [8] have reported measurements that confirm that negligible normal stress differences manifest themselves during the flow of blood[7]. The approach we have followed highlights the efficacy of our model in matching a body of experimental data. A simpler procedure would involve matching the data for normal stress differences (if reliable data were available) as seen, for example, from Equation (62):

$$(S_{zz} - S_{rr}) = 2\left(\nu(\dot{\gamma}_{meas})\lambda_1 - \eta_0\lambda_2\right)\cdot\dot{\gamma}^2_{meas} \qquad (62)$$

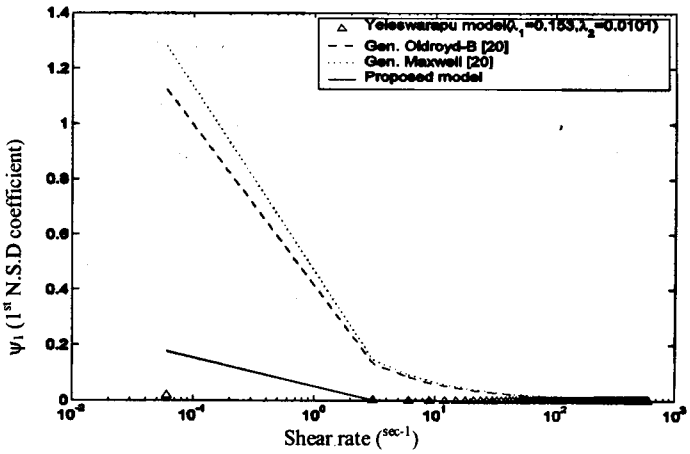

FIGURE 9

First Normal stress difference during the flow of human blood. The predictions of ψ_1, for all the models, are compared. Parameters for the proposed model are the same as in Figure 4; the other models' parameters are those used in Figure 2.

A BRIEF PARAMETER STUDY OF THE YELESWARAPU MODEL [39]

Yeleswarapu ([39], Page 126) observes that the relaxation times are important[8], but also states that his study "is inconclusive with regards to the quantitative effects of viscoelastic behavior of blood since the normal ranges for the constants (λ_1, λ_2) are not known at this stage". The absence of quantitative information regarding λ_1 and λ_2 was, thus far, a shortcoming of Yeleswarapu's model. We shall show that λ_1 and λ_2 have a significant influence on the model predictions (the effect of λ_1, λ_2 in Yeleswarapu's model on the predictions, under pulsatile flow conditions for instance, was, thus far, not documented).

[7] This observation is corroborated by the predictions of the first normal stress difference coefficient (ψ_1) for the various models which show a steep drop in the normal stress difference at shear rates above 1 sec^{-1} (Figure 9) with the model proposed here and that proposed by Yeleswarapu predicting negligible normal stress difference in the entire range of shear rates studied.

[8] See [39] for a parametric study of the Classical Oldroyd-B model, as also the effect of choice of the relaxation times on the velocity profiles and mean flow rates (Figures 25, 37, and 47 in [39]).

The procedure to fix λ_1, λ_2 has already been outlined. The results in Figures 10, 11, 12 and 13 highlight the variations in mean flow rate, wall shear stress, phase differences and velocity profiles, for some choices of λ_1 and λ_2 (ρ = 1050 kg/m^3, R = 0.5 mm, Ve = 1mm/sec, and f = 2Hz for this set of simulations, A = 1 in Equation (61)). There is not much variation in the wall shear stresses (Figure 11) for the range of λ_1, λ_2 studied, the wall shear stress being 180° out of phase with the mean flow. There is significant variation in the mean flow rate amplitude (Figure 10) and phase difference (Figures 10 and 12). The velocity profiles in a cycle, for one choice of λ_1, λ_2 are shown in Figure 13.

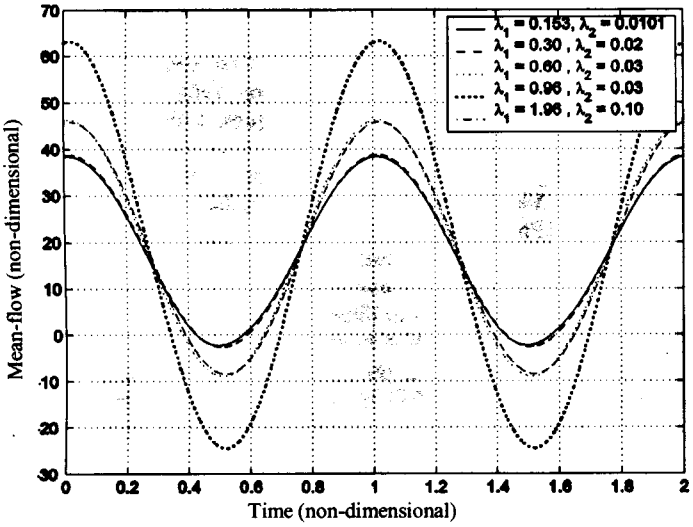

FIGURE 10

Predictions of the mean flow rate using the Yeleswarapu model (for various relaxation times).

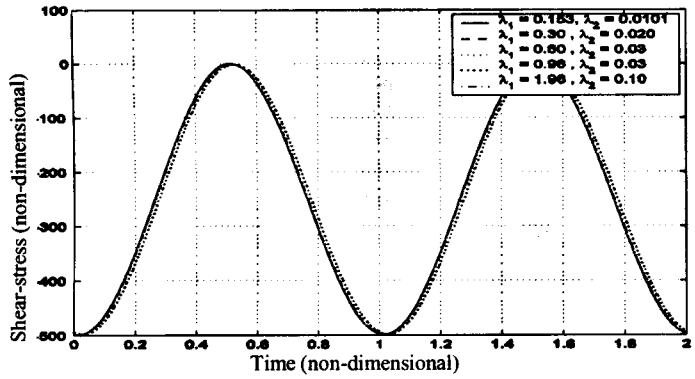

FIGURE 11

Predictions of the wall shear stress using the Yeleswarapu model (for various relaxation times).

ACKNOWLEDGEMENTS

We thank the National Energy Technology Laboratory of the U.S. Department of Energy for its support of this work through the University Partnership Program.

REFERENCES

1. Bureau, M, J Healy, D Bourgoin, M Joly. Etude Experiméntale *In Vitro* du Comportement Rhéologie du Sang et Régime Transitoire à Faible Vitesse de Cisaillement. Rheol Acta 1978; 17:612-625

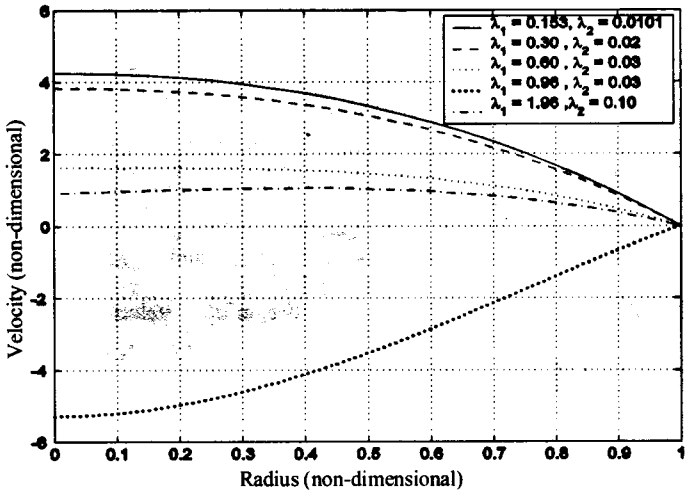

FIGURE 12

Predictions of velocity profiles at θt = 240° using the Yeleswarapu model (for various relaxation times).

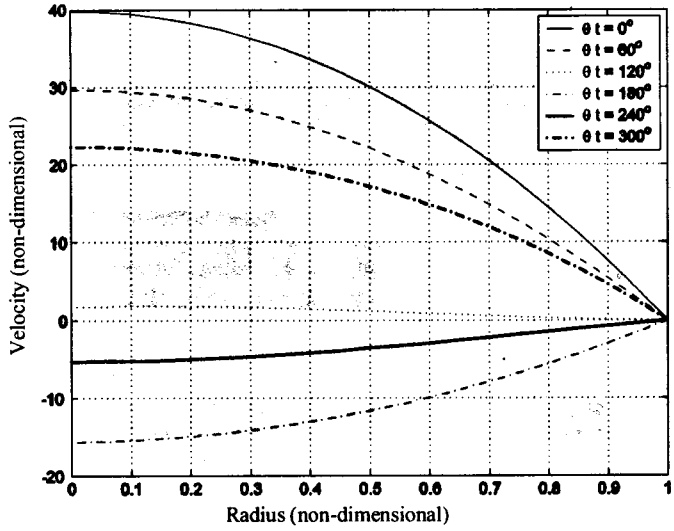

FIGURE 13

Velocity profiles at various instants in a cycle for the Yeleswarapu model (λ_1=0.96 s, λ_2=0.03 s).

2. Bureau, M, J Healy, D Bourgoin, M Joly. Rheological Hysteresis of Blood at Low Shear Rate. Biorheology 1980; 17:191-203
3. Burgreen, GW, JF Antaki, ZJ Wu, AJ Holmes. Computational Fluid Dynamics as a Development Tool for Rotary Blood Pumps. Artif Organs 2001; 25(5):336-340
4. Chien, S, S Usami, RJ Dellenback, MI Gregersen. Blood Viscosity: Influence of Erythrocyte Deformation. Science 1967; 157(3790):827-829
5. Chien, S, S Usami, RJ Dellenback, MI Gregersen. Blood Viscosity: Influence of Erythrocyte Aggregation. Science 1967; 157(3790):829-831
6. Chien, S, RG King, R Skalak, *et al.* Viscoelastic Properties of HUman Blood and Red Cell Suspensions. Biorheology 1975; 12:341-346
7. Chmiel, H, E Walitza. **On the Rheology of Blood and Synovial Fluids**, Research Studies Press, New York, 1980
8. Copley, AL, RG King. On the Viscoelasticity of Anticoagulated Whole Human Blood in Steady Shear as Tested by Rheogoniometric Measurements of Normal Forces. Biorheology 1976; 12:5-10

9. Engeln-Müllges, G, F Uhlig. **Numerical Algorithms with C**. Springer Verlag, Berlin, 1996
10. Gimbrone, MA. Endothelial Dysfunction, Hemodynamic Forces and Atherosclerosis. Thromb Haemostasis 1999; 82(2):722-726
11. Joly, M, C Lacombe, D Quemada. Application of the Transient Flow Rheology to the Study of Abnormal Human Bloods. Biorheology 1981; 18:445-452
12. Kannan, K, IJ Rao, KR Rajagopal. A Thermomechanical Framework for the Glass Transition Phenomenon in Certain Polymers and its Application to Fiber Spinning. J Rheol 2002; 46(4):977-999
13. Kroll, MH, JD Hellums, LV McIntire, *et al.* Platelets and Shear Stress. Blood 1996; 88(5):1525-1541
14. McMillan, DE, NG Utterback, M Nasrinasrabadi, MM Lee. An Instrument to Evaluate the Time Dependent Flow Properties of Blood at Moderate Shear Rates. Biorheology 1986; 23:63-74
15. Murali Krishnan, J, KR Rajagopal. Review of the Uses and Modeling of Bitumen from Ancient to Modern Times. Applied Mechanics Reviews 2003; 56(2):149-214
16. Phillips, WM, S Deutsch. Towards a Constitutive Equation for Blood. Biorheology 1975; 12(6):383-389
17. Pontrelli, G. Pulsatile Blood Flow in a Pipe. Comput Fluids 1998; 27(3):367-380
18. Quemada, D. A Nonlinear Maxwell Model of Biofluids - Application to Normal Blood. Biorheology 1993; 30(3-4):253-265
19. Rajagopal, KR. Multiple Natural Configurations in Continuum Mechanics. Reports of the Institute for Computational and Applied Mechanics 1995
20. Rajagopal, KR, AR Srinivasa. A Thermodynamic Framework for Rate-type Fluid Models. J Non-Newt Fluid Mech 2000; 88:207-227
21. Rajagopal, KR, AR Srinivasa. Modeling Anisotropic Fluids within the Framework of Bodies with Multiple Natural Configurations. J Non-Newt Fluid Mech 2001; 99:109-124
22. Rao, IJ, KR Rajagopal. A Study of Strain-induced Crystallization of Polymers. Int J Solids Struct 2001; 38:1149-1167
23. Rao, IJ, KR Rajagopal. Thermomechanical Framework for the Crystallization of Polymers. Z Angew Math Phys 2002; 53:365-406
24. Schmid-Schönbein, H, R Wells. Fluid Drop-like Transition of Erythrocytes under Shear. Science 1969; 165(3890):288-291
25. Srinivasa, AR. Flow Characteristics of a Multiconfigurational Shear Thinning Viscoelastic Fluid with Particular Reference to the Orthogonal Rheometer. Theor Comput Fluid Dynamics 2000; 5:305-325
26. Sun, N, D DeKee. Simple Shear, Hysteresis and Yield Stress in Biofluids. Can J Chem Engg 2001; 79:36-41
27. Thurston, GB. Viscoelasticity of Human Blood. Biophys J 1972; 12(9):1205-1217
28. Thurston, GB. Frequency and Shear Rate Dependence of Viscoelasticity of Human Blood. Biorheology 1973; 10:375-381
29. Thurston, GB. Elastic Effects in Pulsatile Blood Flow. Microvasc. Res 1975; 9:145-157
30. Thurston, GB. The Effects of Frequency of Oscillatory Flow on the Impedance of Rigid Blood Filled Tubes. Biorheology 1976; 13:191-199
31. Thurston, GB. Rheological Parameters for the Viscosity, Viscoelasticity and Thixotropy of Blood. Biorheology 1979; 16:149-162
32. Thurston, GB. Plasma Release-cell Layering Theory. Biorheology 1989; 9:145-157
33. Thurston, GB. Light Transmission through Blood in Oscillatory Flow. Biorheology 1990; 27:685-700
34. Thurston, GB. Non-Newtonian Viscosity of Human Blood: Flow-induced Changes in Microstructure. Biorheology 1994; 31(2):179-192
35. Vlastos, G, D Lerche, B Koch, *et al.* The Effect of Parallel Combined Steady and Oscillatory Shear Flows on Blood and Polymer Solutions. Rheol Acta 1997; 36:160-172
36. Walters, K, RA, Kemp. On the Use of a Rheogoniometer. Part II: Oscillatory Shear. In: **Polymer Systems: Deformation and Flow**, Proceedings of the 1966 Annual Conference of the British Society of Rheology, Macmillan, London, 1968
37. Whorlow, RW. **Rheological Techniques**, Ellis Horwood Ltd, 1980
38. Womersley, JR. Method for the Calculation of Velocity, Rate of Flow and Viscous Drag in Arteries when the Pressure Gradient is Known. J Physiol 1955; 127:553-563
39. Yeleswarupu, KK. **Evaluation of Continuum Models for Characterizing the Constitutive Behavior of Blood**, PhD Dissertation, University of Pittsburgh, Pittsburgh, PA 1996
40. Yeleswarapu, KK, MV Kameneva, KR Rajagopal, JF Antaki. The Flow of Blood in Tubes: Theory and Experiment. Mech Res Comm 1998; 25(3):257-262

NOMENCLATURE

$B_{\kappa p(t)}$: Left Cauchy-Green stretch tensor calculated using $\kappa_{p(t)}(B)$ as the reference configuration.

$B_{\kappa R}$: Left Cauchy-Green stretch tensor calculated using $\kappa_R(B)$ as the reference configuration.

$C_{\kappa p(t)}$: Right Cauchy-Green stretch tensor calculated using $\kappa_{p(t)}(B)$ as the reference configuration.

$C_{\kappa R}$: Right Cauchy-Green stretch tensor calculated using $\kappa_R(B)$ as the reference configuration.

$F_{\kappa p(t)}$: Deformation Gradient tensor calculated using $\kappa_{p(t)}(B)$ as the reference configuration.

$F_{\kappa R}$: Deformation Gradient tensor calculated using $\kappa_R(B)$ as the reference configuration.

G : Mapping (tensor) between $\kappa_R(B)$ and $\kappa_{p(t)}(B)$.

L : Velocity Gradient tensor calculated using $F_{\kappa R}$ (see text).

r : Coordinate in the radial direction

t : Time

T : Cauchy Stress tensor

v : Velocity vector

W : (elastic) Stored energy function

z : Coordinate in the axial direction

θ : Coordinate in the circumferential direction

Ψ : (specific) Helmholtz potential

ξ : Rate of Dissipation